J Appl Electrochem (2010) 40:855–864
DOI 10.1007/s10800-009-0069-y

ORIGINAL PAPER

Characterization of an electrochemical reactor for the ozone production in electrolyte-free water

Leonardo M. Da Silva · Débora V. Franco · Lindomar G. Sousa · Ismael C. Gonçalves

Received: 15 July 2009 / Accepted: 23 December 2009 / Published online: 13 January 2010

Abstract The filter-press electrochemical ozonizer is characterized as a function of the applied electric current, temperature, and linear velocity of the electrolyte-free water. Lead dioxide electroformed on surface of a non-platinized fine mesh stainless steel support was used as anode. Electrolysis of the electrolyte-free water was carried out using the membrane electrode assembly (MEA) adequately compressed by means of a specially designed clamping system. Electrochemical characterization studies were carried out galvanostatically as a function of temperature and linear velocity of the circulating water. It was verified that the electrochemical ozone production (EOP) taking place at the reacting zones formed at the solid polymer electrolyte (SPE)/mesh electrode interface is not considerably affected by circulating water when the linear velocity inside the distribution channels is higher than 1.20 cm s^{-1}. A current efficiency for the EOP of 13% and a specific electric energy consumption of 70 Wh g^{-1} were obtained when an electric current of 130 A was applied at 30 °C. The reactor service life test revealed that the MEA using the lead dioxide fine mesh electrode as anode and a fine mesh stainless steel electrode as cathode, pressed against the SPE, is stable for the ozone production.

Keywords Electrochemical ozone production · Filter-press reactor · Fine mesh lead dioxide electrode · Zero-gap conditions · Electrolyte-free water

L. M. Da Silva (✉) · D. V. Franco · L. G. Sousa · I. C. Gonçalves
Department of Chemistry, Laboratory of Environmental Electrochemistry, UFVJM, Rodovia MGT 367, km 583, No 5000, Diamantina, MG 39100-000, Brazil
e-mail: lsilvamorais@gmail.com; leonardo.morais@ufvjm.edu.br

1 Introduction

Ozone is an environmentally friendly oxidant used in several applications concerning drinking water and wastewater treatment processes [1–3]. Ozone applications in Integrated Treatment Systems (ITS) accounting for water treatment present at least two important consequences [1–3]: (i) biodegradability increases of the dissolved organics and (ii) introduction of a considerable amount of oxygen in water; thus, creating excellent conditions during the biologically active filtration process.

Ozone is the most powerful disinfectant available capable of oxidizing several different organic pollutants [1–8]. Depending on the dissolved oxygen concentration and the solution pH, the ozone redox potential can be very high (1.51–2.07 V) [1, 2, 6]. Besides, the ozonation process under optimized conditions (e.g., $[O_{3(aq)}]$, contact time, temperature, etc.), alone or combined with hydrogen peroxide (peroxone) and, or UV-light, indeed comprises environmentally friendly technologies for application in water treatment facilities since formation of trihalomethanes during the treatment process is considerably avoided [2, 3].

Ozonation can also be used in the purification of water loops used in the pharmaceutical industry, wood pulp bleaching process, treatment of textile wastewater, etc. [1–3, 6].

Because ozone is a highly reactive gas under ordinary conditions, it has to be generated on site [1–6, 9–13]. In most cases the on site ozone generation is carried out by means of the Dielectric Barrier Discharge (also called Corona Process) [2, 3]. According to the literature [1, 2, 23], the efficiency for ozone generation $(O_2 + O^{\bullet} \rightarrow O_3)$ using the Corona Process depends on the following factors: (i) oxygen source (O_2 or air), (ii) gas temperature, and (iii) presence of impurities in the gaseous phase.

The main drawback presented by the Corona technology is that the energy efficiency decreases rapidly as one tries to increase the ozone generation rate [2]. This inconvenience comes from the fact that ozone decomposition rate by electric spark (silent electric discharge) increases upon increasing the O_3-concentration [1, 6]. From these considerations, several commercial ozonation systems, based on the Corona technology, are commonly designed to generate ozone by operating in the 2–3 wt% or 1–2 wt% range using oxygen or air, respectively. However, in very special cases the O_3-concentration can reach a maximum of ~15 wt% when specially designed dielectric barriers are used [2].

Several different studies revealed that ozone can be alternatively generated by means of the water electrolysis using specially designed electrochemical reactors [1, 2, 4–7, 9–31].

The interest in electrochemical ozone production, EOP, has increased in the last three decades as a consequence of great advances in the research fields of the New Materials Science and Electrochemical Engineering [2, 6, 9, 10, 24]. Nowadays, the EOP process comprises an attractive alternative from the economical point of view for many important ozone applications, as is the case of the ultra-purification of water used in pharmaceutical and semi-conductor industries where the use of ultra-purified water is imperative [2, 6, 9].

The main advantage presented by EOP is the high concentration achieved in the gaseous phase (O_2/O_3), which can range from ~10 up to 35 wt% [2, 4, 9, 29]. As discussed by Da Silva et al. [1, 2, 6], EOP is gaining popularity for small/medium ozone applications due to a couple of features that are not achieved with the Corona technology [1, 2, 6]. For instance, the development of electrochemical reactors operating in electrolyte-free water permitted the direct application of ozone into water streams, thus considerably minimizing the drawbacks associated with the mass transport from gas to the condensed phase (ozone solubilization process) and the release of undesirable by-products (e.g., NO_x in Corona devices) during ozone generation [1, 2, 4, 6, 11–13].

Depending on the ionic conductor used, the electrochemical ozonizers can be classified in two categories [2, 6]: (i) Type-I, where an inert electrode material is immersed in specially designed liquid electrolytes, and (ii) Type-II, where a membrane electrode assembly, MEA, comprising the use of a solid polymer electrolyte, SPE, and gas diffusion or fine mesh electrodes is responsible for electrolysis of the electrolyte-free water under zero-gap conditions.

Reactors classified as Type-II are mainly used for purification and ultra-purification of water [2]. These reactors present the benefit of permitting the micro-bubbles leaving MEA to be directly released into the streaming (treated) water [6, 11, 12]. In addition, the total operational costs can be considerably minimized since very high ozone utilization efficiency can be achieved, and the use of a cooling system is, in principle, not necessary, i.e., these reactors operate at their maximum performance at moderate temperatures (25–35 °C).

Some of the present authors reported previously the characterization of an electrochemical ozonizer where the ozone production was carried out in sulfuric acid solutions using as the anode the lead-dioxide-coating electroformed on surface of a platinized perforated titanium substrate [8]. The present study reports the electrochemical characterization of a filter-press reactor developed using a specially designed MEA to promote the ozone generation from electrolysis of the electrolyte-free water. The lead-dioxide-coating electroformed on surface of a non-platinized fine mesh stainless steel support was used as anode.

2 Experimental

2.1 Preparation of the filter-press electrochemical reactor

2.1.1 Anode

The lead dioxide layer (β-PbO_2) was prepared by electrodeposition at constant current from $Pb(NO_3)_2$ acid solution on the surface of a fine mesh stainless steel support (AISI 304—9 × 10 cm and $\varepsilon = 0.2$ mm), previously etched for 5 min in boiling nitric acid solution (0.5 mol dm^{-3}) to increase the surface roughness via pit formation. β-PbO_2 was then electrodeposited from a solution containing 0.2 mol dm^{-3} $Pb(NO_3)_2$ + 0.01 mol dm^{-3} HNO_3, at 60 °C, using an apparent constant current density of 20 mA cm^{-2} for 1 h. SEM analysis revealed this procedure resulted in a thickness of the β-PbO_2 layer of 90 ± 5 μm.

The final average pore geometry after electrodeposition of β-PbO_2 was mainly characterized by an average cross-section area of 31 × 10^3 μm^2 (see Fig. 1a). An additional mesh stainless steel (AISI 304—$\varnothing = 2.0 \times 2.0$ mm and $\varepsilon = 0.5$ mm) was used to improve the electric contact with the perforated current collector made of stainless steel (see Fig. 2a). Aldrich "purum p.a." products were used throughout.

2.1.2 Cathode

A fine mesh stainless steel (AISI 304—9 × 10 cm) without further treatment was used as cathode, where $\varnothing = 0.05 \times 0.05$ mm and $\varepsilon = 0.05$ mm (see Fig. 1b). An

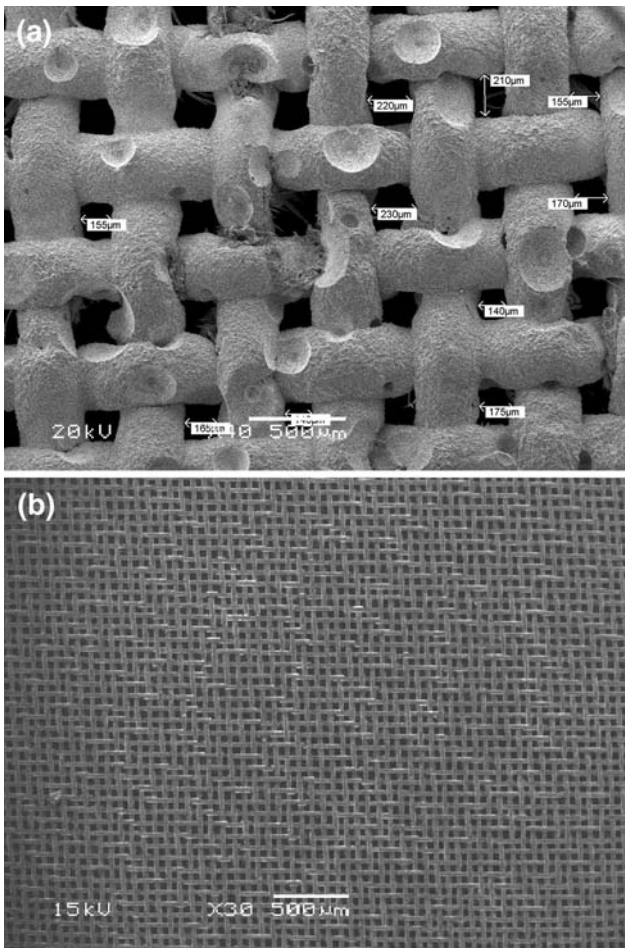

Fig. 1 SEM images obtained for fine mesh electrodes used in membrane electrode assembly: **a** AISI304/β-PbO_2 and **b** AISI304

additional mesh stainless steel (AISI 304—$\varnothing$ = 2.0 × 2.0 mm and ε = 0.5 mm) was used to improve the electric contact with the perforated current collector made of stainless steel.

Figure 1 shows SEM images obtained for fine mesh electrodes used in MEA, while Fig. 2 shows pictures of the cell housing made of acrylic.

2.1.3 MEA

The system comprising electrodes, SPE, and current collectors was assembled using a specially designed cell housing made of acrylic, where fine mesh electrodes were pressed against the SPE (Nafion® 117—Dupont) using a clamping system (see Figs. 2b, 3). Fluid manifolds (water distribution channels) were machined into the intermediate acrylic plates to facilitate the water supply at the SPE/electrode interface (active zones for electrolysis) (see Figs. 2b, 3).

Since the active zones for water electrolysis are formed only at the electrode regions in intimate contact with the SPE/electrode interface, the mechanical tension (pressure) applied upon MEA was controlled to increase the active surface regions for electrolysis by means of fastening spring-loaded screws (clamping system) fixed in the acrylic external wall (ε = 24 mm) (see Figs. 2b, 3). This procedure ensured adequate compression onto the SPE, thus providing the necessary conditions for the zero-gap approach and preventing the membrane rupture.

The specific conductivity presented by the hydrated Nafion® 117 membrane [9, 10, 24] allied with its specific geometry in the present case ($\varepsilon \approx 200$ μm and $A_G = 90$ cm^2) resulted in an apparent conductance, σ^*, of 374 S at 30 °C. Therefore, the apparent SPE resistance, $R^* = 1/\sigma^*$, calculated was 2.7 mΩ.

The resultant prototype for EOP ($I \leq 130$ A) was conceived to obtain an electrochemical ozonizer for small scale applications (up to 5 g h^{-1}). A scheme describing the main components of MEA comprising the filter-press electrochemical ozonizer is presented in Fig. 3.

2.2 Electrochemical characterization

Water electrolysis was carried out under galvanostatic conditions using distilled water ($\sigma \approx 6$ μS at 30 °C), which was circulated using different linear velocities. According to the literature [11, 12, 14, 19], the cell voltage,

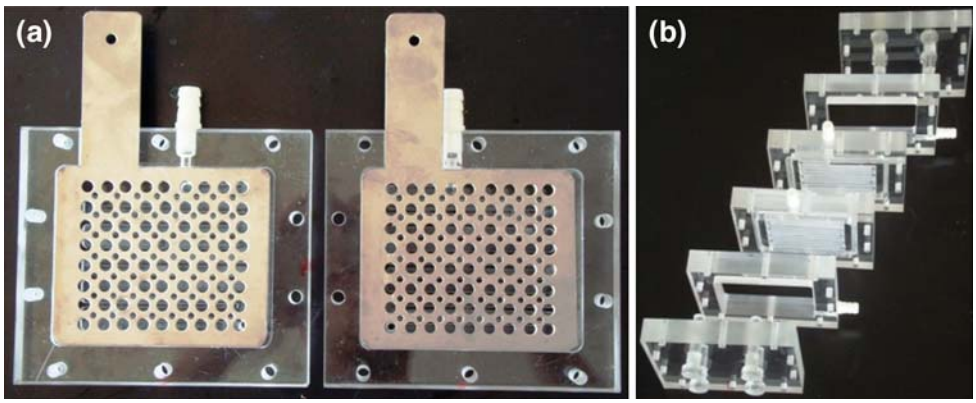

Fig. 2 Pictures of the cell housing made of acrylic: **a** perforated current collectors and **b** expanded view of the different elements comprising the cell housing

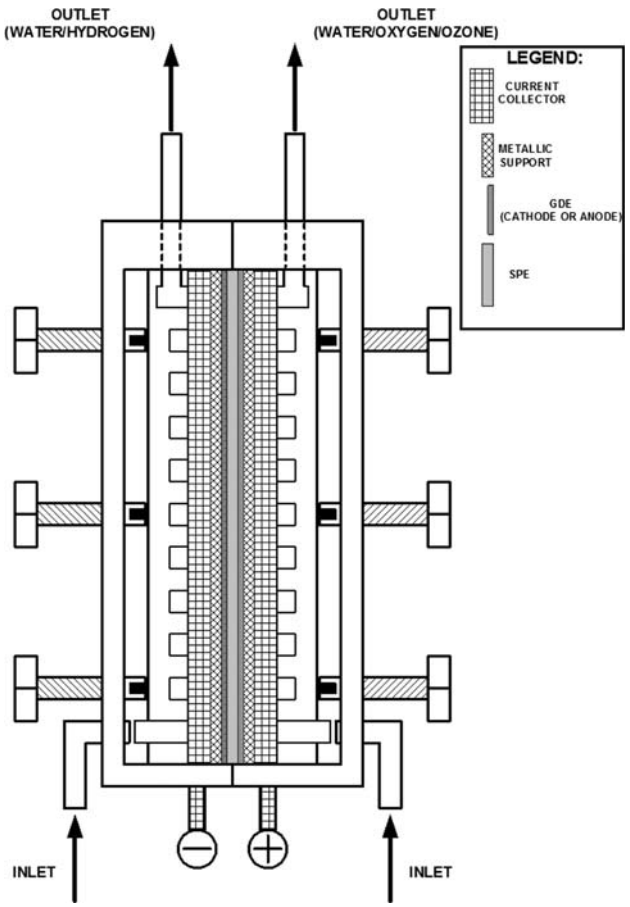

Fig. 3 Scheme describing the main components comprising the filter-press electrochemical ozonizer

U, and the EOP current efficiency, Φ_{EOP}, present a transient behavior; i.e., U and Φ_{EOP} increases asymptotically up to stationary values for a given applied current, I, and temperature, T. Therefore, before each run the as-prepared MEA system was pre-polarized (15 A and 30 min) to ensure stationary conditions. After that, for each applied current higher than 15 A, a conditioning time of 10 min was adopted to read the steady state absorbance in gaseous phase.

After saturation of the circulating water with the anodic gas mixture (O_2/O_3), the ozone concentration in gaseous phase was measured by UV absorption at 254 nm using a homemade gas flow cell [8]. This procedure was conducted as function of the applied current (15–130 A) and water temperature (10–40 °C).

EOP partial current, I_{EOP}, and EOP current efficiency, Φ_{EOP}, were calculated using Eqs. 1 and 2, respectively [8]:

$$I_{EOP}(\mathrm{A}) = AGzF/\varepsilon l \quad (1)$$

$$\Phi_{EOP}(\mathrm{wt\%}) = I_{EOP}/I_T \quad (2)$$

where A is the absorbance at 254 nm, G is the volumetric flow rate of ($O_2 + O_3$) ($dm^3\ s^{-1}$), z is the number of electrons (=6), ε is the ozone absorptivity at 254 nm (3024 $cm^{-1}\ mol^{-1}\ dm^3$ [23]), l is the optical path length (0.63 cm) [8], I_T is the total current (A), and $F = 96485\ C\ mol^{-1}$.

EOP specific electric energy consumption, P^o_{EOP}, was calculated using Eq. 3 [8]:

$$P^o_{EOP}\left(\mathrm{Wh\ g^{-1}}\right) = UzF/1.73 \times 10^5 \Phi_{EOP}, \quad (3)$$

where U is the cell voltage.

The reactor performance for EOP was also evaluated using the extensive parameters defined as: (i) ozone production rate, v_{EOP}, and (ii) gain of ozone mass per total power consumption, ϑ_{EOP}, which were calculated using Eqs. 4 and 5, respectively [8]:

$$v_{EOP}\left(\mathrm{gh^{-1}}\right) = 3600\, I_{EOP} M/zF \quad (4)$$

$$\vartheta_{EOP}\left(\mathrm{gW^{-1}\ h^{-1}}\right) = v_{EOP}/I_T U, \quad (5)$$

where M is the ozone molecular weight (48 g mol^{-1}).

Figure 4 shows a scheme of the experimental setup used in the characterization study of the electrochemical ozonizer.

The electrochemical reactor was powered using a 150 A/10 V d.c. current source from TECTROL (Brazil). A model 77601-10 MASTERFLEX peristaltic pumps (Cole-Parmer) were used to circulate distilled water inside the anodic and cathodic compartments at different volumetric flow rates to obtain the desired linear fluid velocities (1.15–1.40 cm s^{-1}).

Temperature control was performed using heat exchangers connected to the all-glass water reservoir/gas separator flasks. Temperature of the circulating water was monitored using digital thermometers.

While the anodic gaseous mixture (O_2/O_3) was treated for safety precautions using the 2.0 wt% KI solution before its release in the atmosphere to avoid contamination of the air, the cathodic gas (H_2) was spontaneously discarded without further precautions.

3 Results and discussion

3.1 Influence of the linear fluid velocity on polarization behavior

Different apparent current densities (0.15–1.3 A cm^{-2} - A_G = 90 cm^2) were applied to the reactor as functions of the linear velocity of the fluid (water), v, to study the influence of the fluid dynamics inside the distribution channels on polarization behavior. In all cases, the Reynolds number calculated as function of the linear velocity of the fluid was higher than 3000, indicating a turbulent hydrodynamic regime [10, 24].

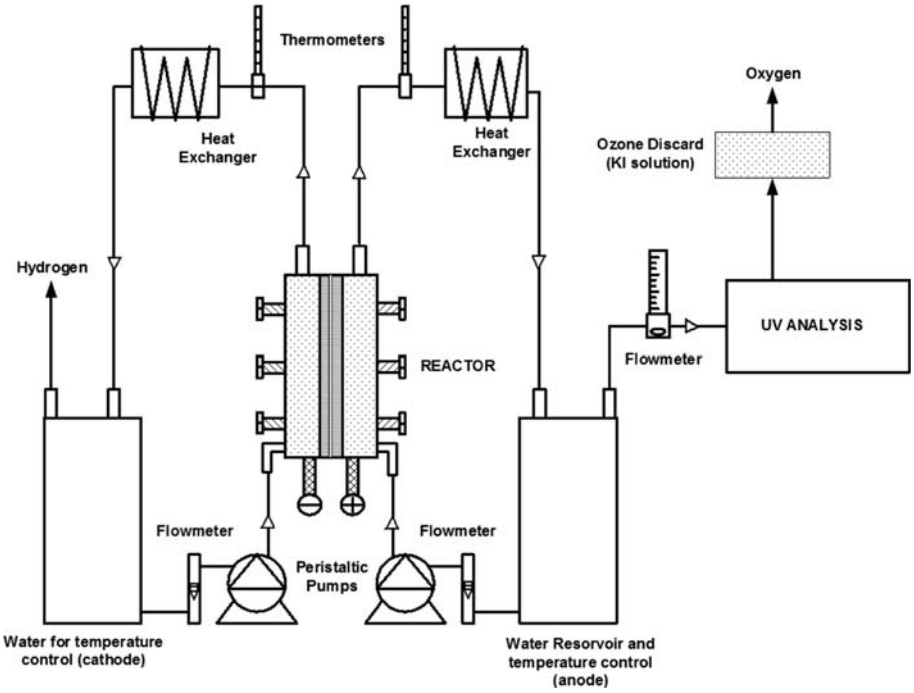

Fig. 4 Scheme of the experimental setup used in the characterization study of the electrochemical ozonizer

Figure 5 shows polarization curves, U versus I, uncorrected for ohmic drop recorded as function of the linear velocity of the circulating water, v, at 30 °C.

Analysis of Fig. 5 reveals that only minor changes in polarization behavior take place at $v > 1.20$ cm s^{-1}, thus indicating that turbulent conditions have only a minor effect on electrolysis taking place at the active zones formed at the SPE/electrode interface.

In principle, in the case of electrochemical ozonizers using electrolyte solutions, all regions of the electrode surface area are available for water electrolysis [8]. On the contrary, in the case of filter-press reactors based on the SPE approach, the electrolysis using electrolyte-free water can only proceed at the active interface regions, where an intimate contact is established between the fine mesh electrodes and the SPE [2].

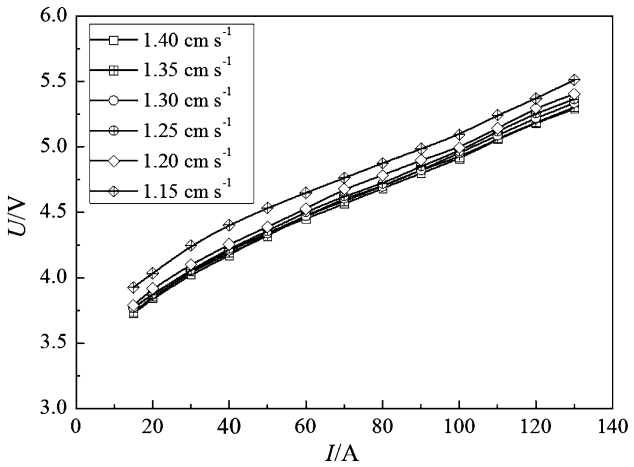

Fig. 5 Polarization curves, U vs. I, uncorrected for ohmic drop recorded as function of the linear velocity of the circulating water, v, at 30 °C

Figure 6 presents a scheme representing the MEA and the fundamental processes taking place at the anodic reaction zones.

According to Fig. 6, in order to carry out electrolysis of the electrolyte-free water, the MEA must furnish conditions to ensure the adequate electronic and ionic conductions. Therefore, the contact area ratio of mesh electrode to a unit area of SPE must be adequate (e.g., 0.30–0.60 [19]) to maximize the surface concentration of the active centers for electrolysis, thus decreasing the apparent decomposition potential (see further discussion).

Figure 6 shows that water circulating in a fluid distribution channel must cross the porous structure of the anode to reach the active surface zone located at the SEP/electrode interface, while the gaseous products (O_2 and O_3) must escape from the porous anode structure to permit water replacement at the reaction sites.

According to the literature [11, 12], the hydrodynamic properties of the fluid circulating inside the fluid distribution channel and the fluid percolating the porous electrode structure can be rather different due to a reduction in convection lines [10–12]. On the other hand, several studies show that turbulent conditions inside the porous electrode structure can be induced when gas evolution reactions take place [24, 32, 33], since in this case the bubble generation process constantly creates pressure fluctuations inside the porous regions.

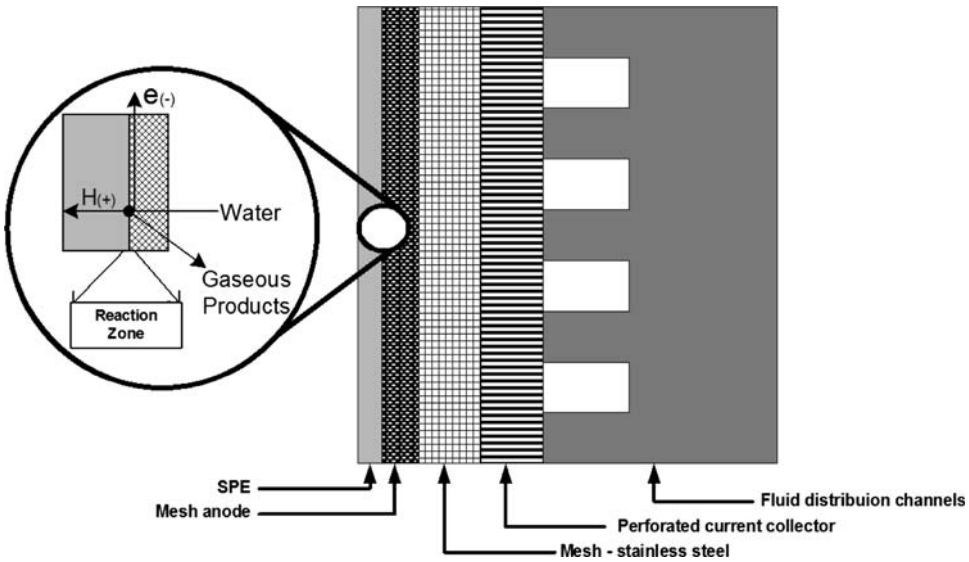

Fig. 6 Scheme representing the membrane electrode assembly and the fundamental processes taking place at the anodic reaction zones

From the above considerations, it is worth mentioning that the hydrodynamic regime evaluated from linear velocity of the circulating water inside the distribution channels does not reflect the "true" hydrodynamic regime at the vicinity of the reaction zones, since in this case the pattern of convection lines at the reaction zones is unknown.

3.2 Influence of temperature on cell voltage and apparent decomposition potential

Different cell components can be, at least in principle, manipulated to reduce ohmic losses [34]. The most important among them are [10, 24]: (i) thickness and cross-section area of the conductive cell layers, (ii) intrinsic conductivities and the effective conductance of these materials, and (iii) effective contact area established at the SPE/electrode interface.

The heat dissipated at the anode side is of prime concern because of the sensitivity of ozone current efficiency on temperature [11, 12, 15, 19]. According to the literature [13, 34], the overall rate of heat dissipation is governed by a complex process comprising the heat transfer through the metallic components of the MEA and by the leaving gas products.

From the above considerations, a study was carried out to investigate the influence of water temperature on cell voltage at 1.35 cm s^{-1}. Figure 7 shows the polarization behavior, U versus I, uncorrected for ohmic drop, exhibited by the filter-press reactor and the dependence of the apparent decomposition potential, U_o, on temperature, T, at 1.35 cm s^{-1}.

Analysis of Fig. 7a reveals that U decreases slightly on increasing T. Also verified is that the U versus I profile is practically linear for $I \geq 50$ A. This behavior was also verified by other authors [11, 12, 15]. Based on these experimental findings, it can be argued that the phenomenon governing the cell potential is the total ohmic drop across the MEA (e.g., non-ideal mechanical contact between the different materials, SPE resistance, etc.) [10, 24, 34].

The voltage distribution in the present case is described by Eq. 6 [24]:

$$U = U_0 + \Sigma|\eta| + IR_\Omega, \tag{6}$$

where U_0 is the apparent decomposition potential at $I \rightarrow 0$, η is the overpotential (activation and/or polarization), and R_Ω is the specific resistance of the MEA.

Equation 6 can be analyzed in two limited cases: (i) low-current domain ($U \approx U_0 + \sum|\eta|$) and (ii) high-current density domain ($U \approx U_0 + IR_\Omega$). Therefore, it can be expected that application of low currents will result in non-linear polarization profiles (see Fig. 7a, $I < 50$ A), while application of high currents will lead to a linear (ohmic) behavior (see Fig. 7a, $I \geq 50$ A).

From the above considerations, the polarization behavior in the high-current domain can be described by the linear approximation described by Eq. 7 [24]:

$$U \cong U_0 + IR_\Omega, \tag{7}$$

The linear regression analysis ($r > 0.997$) furnished a constant resistance of 12 mΩ, since the polarization curves are parallel for the different temperatures. As expected, due to presence of the different ohmic components, the total MEA resistance is indeed higher than the specific SPE resistance of 2.7 mΩ (see Sect. 2.1).

Analysis of the experimental findings presented in Fig. 7b revealed a good linear correlation between U_0 and T, which furnished the temperature coefficient relation described by Eq. 8:

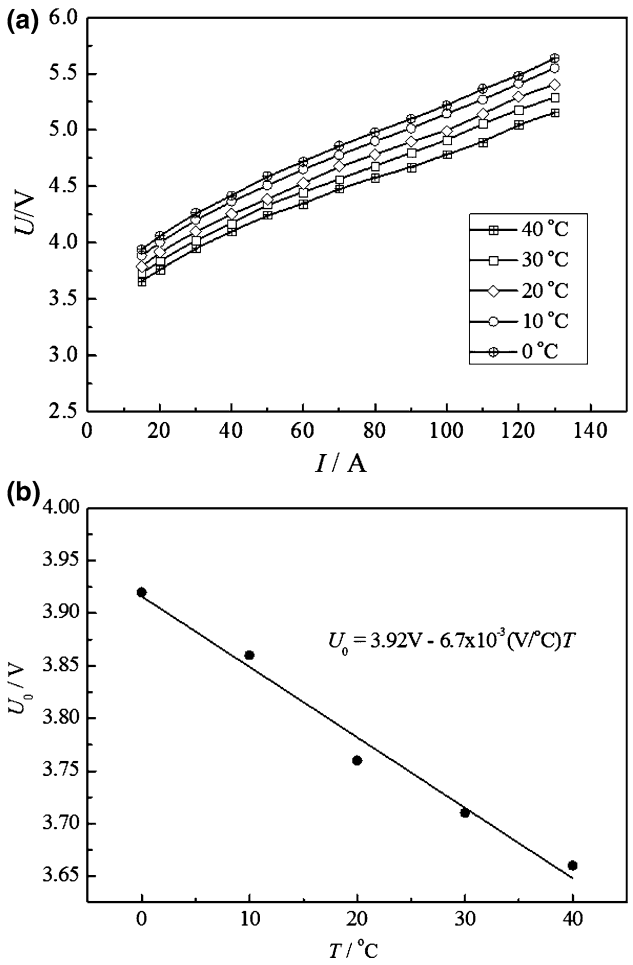

Fig. 7 Polarization behavior: **a** polarization profiles, U vs. I, uncorrected for ohmic drop as function of the temperature and **b** dependence of the apparent decomposition potential, U_o, on temperature, $v = 1.35$ cm s^{-1}

$$U_0(\mathrm{V}) = 3.92\mathrm{V} - 6.7 \times 10^{-3}\mathrm{V}^0\mathrm{C}^{-1}T(^\circ\mathrm{C}) \quad (8)$$

As a result, the experimental correlation for cell voltage in the high current domain is represented by Eq. 9:

$$U(\mathrm{V}) = 3.92\mathrm{V} - 6.7 \times 10^{-3}\mathrm{V}^0\mathrm{C}^{-1}T(^\circ\mathrm{C}) + 12 \times 10^{-3}\mathrm{VA}^{-1}I(\mathrm{A}) \quad (9)$$

Analysis of Eq. 9 reveals that a decrease in cell voltage to reduce the specific electric energy consumption for EOP requires reduction in the apparent decomposition potential (e.g., increase in the active regions for electrolysis, reduction in the cathode overpotential, etc.) and/or minimization of the ohmic components (e.g., better electric contacts between the different components of MEA, etc.) [34].

From the above considerations, it can be argued that optimization of the electrodeposition conditions concerning preparation of the β-PbO_2 layer to promote reduction of the average hole size, which is large in comparison with the holes presented by the mesh cathode (see Fig. 1) can result in reduction in U_0 values due to a reduction in charge transfer resistance [5].

3.3 Influence of temperature and electric current on current efficiency for EOP

Figure 8 shows the dependence of the EOP current efficiency, Φ_{EOP}, on temperature of the circulating water, T, and the applied electric current, I.

In agreement with the literature [11, 12, 15], it was verified that Φ_{EOP} increases on increasing I, reaching a maximum of 13% at 130 A and 30 °C. A comparison of these findings with the literature reports [2, 9, 18] revealed the current efficiency for EOP presented by the reactor using mesh electrodes is acceptable for practical purposes, since some of the commercially available electrochemical ozonizers operate presenting a current efficiency of ~14% [2, 10].

As discussed by Stucki et al. [11, 12], Φ_{EOP} reaches a plateau above ~1.3 A cm^{-2}, while the optimum for the specific electric energy consumption lies at ~1.0 A cm^{-2}. However, a critical review of the literature revealed that the maximum Φ_{EOP} value (plateau) is indeed system-dependent [11, 12, 14, 15, 17–22]. A plausible explanation for the influence of MEA on Φ_{EOP} can be provided taking into account the electrode mechanism reported previously for the simultaneous production of oxygen and ozone using inert electrodes [5, 27–30]. In this case, changes regarding Φ_{EOP} can be correlated to the physico-chemical properties of the SPE/mesh anode interface, which govern the surface concentration of the reaction zones and the active concentration of the oxygenated species [5].

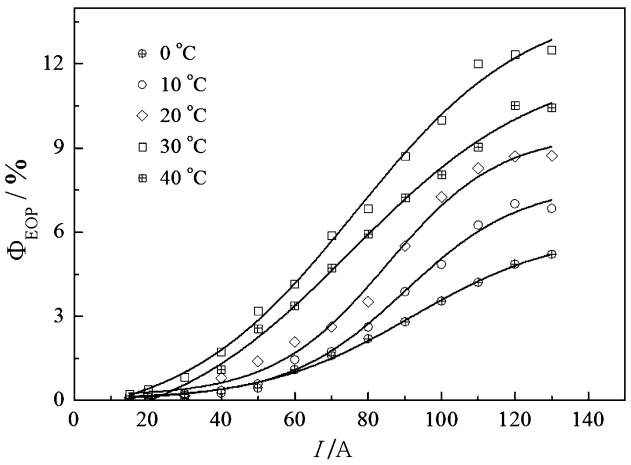

Fig. 8 Dependence of the current efficiency for the electrochemical ozone production, Φ_{EOP}, on applied electric current, I, and temperature, T, at 1.35 cm s^{-1}

The theoretical analysis presented by Da Silva et al. [28–30] for the electrode mechanism concerning the O_2/O_3 production indicates that a set of different partial surface coverages by atomic and molecular oxygen species can be ascribed to the same Φ_{EOP} value. In light of these considerations, it can be supposed that the physico-chemical properties of the SPE/mesh anode interface can be, at least in principle, modulated to increase the nucleation sites for ozonation; i.e., increase in surface concentration of the active centers where the surface reaction $O_{2(ads.)} + O^{\bullet}_{(ads.)} \rightarrow O_{3(ads.)}$ takes place [2, 5, 27].

3.4 Influence of the fluid dynamics on current efficiency for EOP

Figure 9 shows the dependence of the current efficiency for the EOP, Φ_{EOP}, and cell voltage, U, on linear velocity of the circulating water, v, for an applied current of 100 A.

Analysis of Fig. 9 reveals that Φ_{EOP} and U become independent of the hydrodynamic conditions at $v \geq 1.25$ cm s^{-1}. These findings are in agreement with the literature [11, 12], where it was reported that Φ_{EOP} is affected by fluid dynamics only below a threshold v value.

According to the literature [11, 12], changes concerning Φ_{EOP} and U at lower linear velocities of the circulating water ($v < 1.25$ cm s^{-1}) can be correlated with the elementary processes governing bubble removal and heat dissipation at the SPE/anode interface. In this context, the decrease in current efficiency presented in Fig. 9 at lower linear velocities can be attributed to thermal ozone decomposition caused by inefficient heat removal at the interface region [17–19], while the concomitant increase in cell voltage can be correlated to the increase in interfacial ohmic resistance, which is caused by inefficient removal of the bubbles adhered at the SPE/electrode interface provided by the convection lines of the circulating fluid.

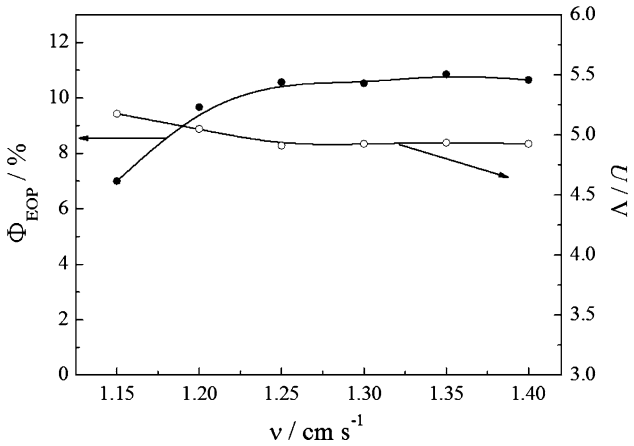

Fig. 9 Dependence of the current efficiency for the electrochemical ozone production, Φ_{EOP}, and cell voltage, U, on linear velocity of the circulating water, v. Conditions: $T = 30$ °C and $I = 100$ A

3.5 Specific electric energy consumption and ozone production rate: influence of temperature and electric current

In many cases, the reactor performance for EOP is not adequately evaluated from the point of view of Electrochemical Engineering; i.e., current efficiency versus ozone production rate, electrode stability, scale-up possibilities, etc. [10, 24]. In fact, an electrochemical ozonizer can present a high-current efficiency for EOP without, however, presenting moderate/high space time yield values and/or moderate/low values for the specific electric energy consumption.

From the above considerations, the evaluation of the overall reactor performance for EOP was carried out in the present study taking into account the intensive and extensive reactor parameters previously described in the literature [8, 11–15].

Figure 10 shows the dependence of the specific electric energy consumption for the EOP, P^{o}_{EOP}, and the ozone production rate, v_{EOP}, on applied electric current, I, and temperature, T.

Analysis of Fig. 10a reveals that P^{o}_{EOP} values considerably decrease upon increasing the applied electric current. The non-linear behavior presented in Fig. 10 is dictated by Eq. 3 ($P^{o}_{EOP} \propto 1/\Phi_{EOP}$), where the correlation for current efficiency, $\Phi_{EOP}(I, T)$, is obtained experimentally [5].

These experimental findings reveal the important influence of T and I on P^{o}_{EOP}, where a minimum value of 70 Wh g^{-1} for the specific electric energy consumption was found at $I > 110$ A and 30 °C. A review of the literature [11, 12, 15, 19] revealed that P^{o}_{EOP} values obtained for filter-press electrochemical ozonizers using gas diffusion or mesh electrodes change from ~58 up to 75 Wh g^{-1} for current densities of ~1.5 A cm^{-2}.

Analysis of Fig. 10b reveals that the ozone production rate considerably increases upon increasing the applied electric current. In addition, it was verified that the ozone production reaches a maximum rate at ~30 °C. According to these findings, the electrochemical ozonizer using mesh electrodes can produce up to 5 g h^{-1} through the expense of a specific electric energy consumption of 70 Wh g^{-1}.

Several studies revealed that a small ozone dosage of ~0.5–2.0 ppm is sufficient to promote purification or ultra-purification of water for different purposes (e.g., pharmaceutical and electronic industries, water bottling process, etc.) [2, 3]. Therefore, rationalization of the literature reports [2, 3, 6, 11, 12] permits proposing that the present ozone production rate (see Fig. 10) is compatible

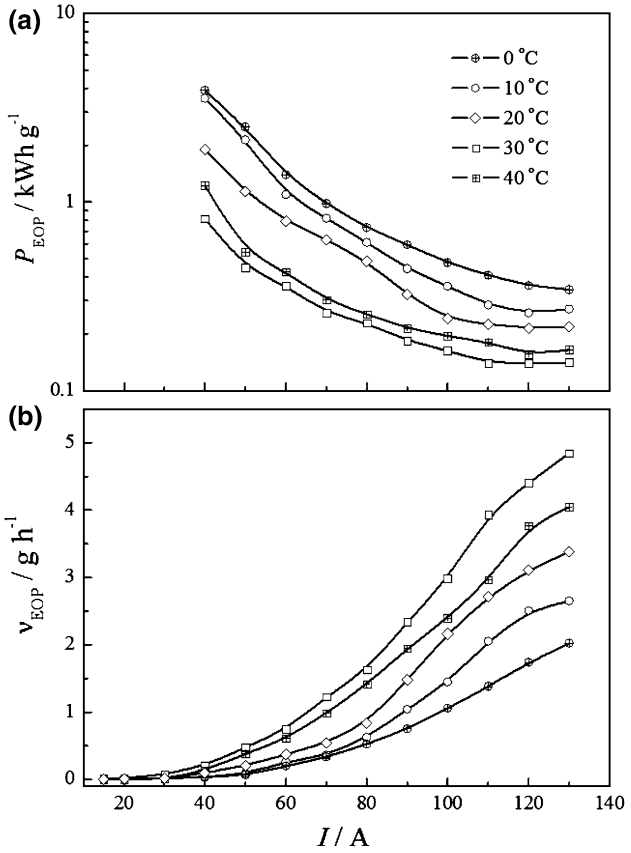

Fig. 10 Dependence of the specific electric energy consumption for the electrochemical ozone production, P^{o}_{EOP}, and the ozone production rate, v_{EOP}, on applied electric current, I, and temperature, T, at 1.35 cm s^{-1}

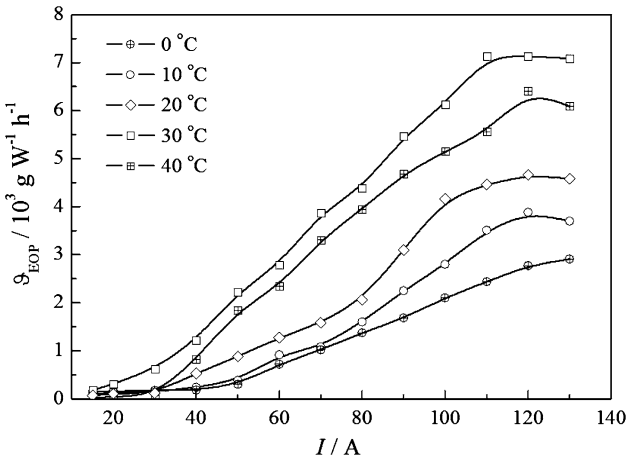

Fig. 11 Dependence of the gain of ozone mass per total power consumption, ϑ_{EOP}, on the applied electric current, I, and temperature, T, at 1.35 cm s^{-1}

with the ozone demand required to treat ~2500–10000 dm^3 of water per hour.

Figure 11 shows the dependence of the gain of ozone mass per total power consumption, ϑ_{EOP}, on the applied electric current and temperature. Considering that ϑ_{EOP} takes into account the total energy demand due to ohmic losses and overpotentials (anodic and cathodic), it can be concluded from these findings that the best overall reactor performance for ozone production is obtained at higher currents (110–130 A) applied at 30 °C.

3.6 Reactor stability under long-term electrolysis

The reactor stability for the simultaneous production of oxygen and ozone was evaluated, recording the cell voltage and current efficiency for the EOP process, during a long-term electrolysis carried out during 30 days ($I = 100$ A, $T = 30$ °C, and $v = 1.35$ cm s^{-1}).

It was found in this study that cell voltage and current efficiency for EOP do not suffer changes during the long-term electrolysis ($U = 4.5 \pm 0.1$ V and $\Phi_{EOP} = 12.0 \pm 0.2$ wt%). Analysis of these findings revealed that the MEA developed for ozone production from electrolysis of the electrolyte-free water, using as the anodic material the lead-dioxide-coating electroformed on surface of a non-platinized mesh stainless steel support, is stable in the prevailing experimental conditions.

According to the literature [12, 19], the stability presented by the lead dioxide coating (β-PbO_2) in the filter-press reactor during the electrolysis of the electrolyte-free water at very high current densities (drastic electrolysis conditions) is by virtue of the absence/minimization of convection at the active regions of the SPE/anode interface (f.i., see model in Fig. 6). In this case, the precipitated β-PbO_2 phase at the active surface regions of the MEA is redeposited immediately on the active zones for electrolysis located at the SPE/anode interface, thus constantly regenerating the active layer [12, 19].

In light of the discussion presented in Sect. 3.1, it can be proposed that convection imposed by bubble generation inside the porous electrode structure does not reach to a considerable extent the intimate contact regions established at the SPE/anode interface where regeneration of the active layer takes place [11, 12].

4 Conclusions

The MEA, using the lead-dioxide-coating electroformed on the surface of a non-platinized fine mesh stainless steel support, was successful in providing experimental conditions for the EOP from electrolysis of the electrolyte-free water.

According to the experimental conditions adopted, based on the zero-gap approach, it was verified that active zones for electrolysis are formed at the SPE/electrode

interface by means of an adequate compression of the MEA using the clamping system.

Polarization studies carried out as a function of the temperature of the circulating water revealed that cell voltage decreases slightly upon increasing the temperature. It was also found that cell voltage at high applied currents is governed by the total ohmic drop across the MEA. This study permitted us to determine the apparent decomposition potential and the temperature coefficient for cell voltage.

The study concerning the influence of the linear velocity of the circulating water inside the distribution channels on the reactor performance for ozone production revealed that current efficiency and cell voltage become independent of linear velocity above 1.25 cm s^{-1}.

The study concerning ozone production as a function of temperature, linear velocity of the fluid, and the applied electric current, revealed a maximum efficiency for the ozonation process of 13% at 130 A and 30 °C, which corresponds to an ozone production rate of 5 g h^{-1}. Also obtained in this study was a minimum value for the specific electric energy consumption of 70 Wh g^{-1} when the maximum current efficiency of 13% is considered.

The long-term electrolysis carried out during 30 days revealed that cell voltage and current efficiency do not suffer changes during the electrolysis, thus revealing the MEA developed in the present work is stable for the ozone production process.

The experimental findings revealed that the EOP process is a promising alternative technology for small ozone applications where the use of the Corona process is not recommended, as in the case of the ultra-purified water required by the pharmaceutical and semiconductor industries.

Acknowledgment L. M. Da Silva wishes to thank the FAPEMIG Foundation.

References

1. Da Silva LM, Jardim WF (2006) Quim Nova 29:310
2. Da Silva LM, Franco DV, Gonçalves IC, Sousa LG (2009) In: Gertsen N, Sonderby L (eds) Water purification. Nova Science Publishers Inc, New York
3. Tchobanoglous G, Burton FL, Stensel HD (2003) Wastewater engineering: treatment and reuse, 4th edn. Metcalf & Eddy Inc., New York
4. Tatapudi P, Fenton JM (1994) In: Sequeira CAC (ed) Environmental oriented electrochemistry. Elsevier, Amsterdam
5. Da Silva LM, De Faria LA, Boodts JFC (2003) Electrochim Acta 48:699
6. Franco DV, Jardim WF, Boodts JFC, Da Silva LM (2008) CLEAN 36:34
7. McKenzie KS, Sarr AB, Mayura K, Bailey RH, Miller DR, Rogers TD, Norred WP, Voss KA, Plattner RD, Kubena LF, Phillips TD (1997) Food Chem Toxicol 35:807
8. Da Silva LM, Franco DV, Forti JC, Jardim WF, Boodts JFC (2006) J Appl Electrochem 36:523
9. Scott K (1995) Electrochemical processes for clean technology. The Royal Society of Chemistry, Cambridge
10. Pletcher D, Walsh FC (1990) Industrial electrochemistry, 2nd edn. Chapman and Hall, London
11. Stucki S, Theis G, Kötz R, Devantay H, Christen H (1985) J Electrochem Soc 132:367
12. Stucki S, Baumann H, Christen H, Kötz R (1987) J Appl Electrochem 17:773
13. Foller PC, Kelsall GH (1993) J Appl Electrochem 23:996
14. Babak AA, Fateev VN, Amadelli R, Potapova GF (1994) Russ J Electrochem 30:739
15. Katoh M, Nishiki Y, Nakamatsu S (1994) J Appl Electrochem 24:489
16. Foller PC, Goodwin ML (1984) Ozone: Sci Eng 6:29
17. Arihara K, Terashima C, Fujishima A (2007) J Electrochem Soc 154:E71–E75
18. Sang-Do H, Duk KJ, Singh KC, Chaudhary RS (2004) Ind J Chem 43:1599
19. Onda K, Ohda T, Kusonoki H, Takezawa S, Sunakawa D, Araki T (2005) J Electrochem Soc 152:177
20. Wang YH, Cheng S, Chan KY (2006) Green Chem 8:568
21. Kraft A, Stadelmann M, Wünsche M, Blaschke M (2006) Electrochem Commun 8:883
22. Awad MI, Sata S, Kaneda K, Ikematsu M, Okajima T, Ohsaka T (2006) Electrochem Commun 8:1263
23. Rice RG, Netzer A (eds) (1982) Handbook of ozone technology and applications, vol 1. Ann Arbor Science, Ann Arbor
24. Wendt H, Kreysa G (1999) Electrochemical engineering: science and technology in chemistry and other industries. Springer, Berlin
25. Wabner DW, Grambow C (1985) J Electroanal Chem 195:95
26. Babak AA, Amadelli R, De Battisti A, Fateev VN (1994) Electrochim Acta 39:1597
27. Da Silva LM, Franco DV, De Faria LA, Boodts JFC (2004) Electrochim Acta 49:3977
28. Da Silva LM, De Faria LA, Boodts JFC (2001) Pure Appl Chem 73:1871
29. Da Silva LM, De Faria LA, Boodts JFC (2003) Quim Nova 26:880
30. Franco DV, Da Silva LM, Jardim WF, Boodts JFC (2006) J Braz Chem Soc 17:746
31. Kötz ER, Stucki S (1987) J Electroanal Chem 228:407
32. Chirkov YG (2000) Elektrokhimiya 36:526
33. Maslii AI, Poddlubnyi NP (1996) Elektrokhimiya 32:1006
34. Sundmacher K, Rihko-Struckmann LK, Galvita V (2005) Catal Today 104:185